

### Public Domain Mark 1.0 Universal

This work was written as part of one of the author's official duties as an Employee of the United States Government and is therefore a work of the United States Government. In accordance with 17 U.S.C. 105, no copyright protection is available for such works under U.S. Law.

Access to this work was provided by the University of Maryland, Baltimore County (UMBC) ScholarWorks@UMBC digital repository on the Maryland Shared Open Access (MD-SOAR) platform.

### **Please provide feedback**

Please support the ScholarWorks@UMBC repository by emailing [scholarworks-group@umbc.edu](mailto:scholarworks-group@umbc.edu) and telling us what having access to this work means to you and why it's important to you. Thank you.

## Physically based classification and satellite mapping of biophysical characteristics in the southern boreal forest

Forrest G. Hall

NASA Goddard Space Flight Center, Greenbelt, Maryland

David E. Knapp and Karl F. Huemmrich

Hughes STX, Goddard Space Flight Center, Greenbelt, Maryland

**Abstract.** Fundamental problems inherent to the existing land cover and biophysical characteristic algorithms are fourfold: (1) their failure to deal physically with global and interannual variations in surface reflectance arising from Sun and view angle variations, (2) decoupling of the land cover classification algorithm from the biophysical characteristic inference algorithm with no ability to control biophysical parameter estimation error arising from misclassification, (3) invalid statistical assumptions within classification algorithms used to model reflectance distribution functions, and (4) sole reliance on vegetation indices that can limit performance for several major land cover classes. To address these problems, we develop an integrated, physically based classification and biophysical characteristics estimation algorithm that utilizes canopy reflectance models to account directly for signature variations from Sun angle, topographic, and other variations. Our approach fuses into a single algorithm both land cover classification and biophysical characteristics estimation, permitting one set of physically based canopy reflectance models to be used for both. The use of canopy reflectance models eliminates the need for unrealistic assumptions, such as multivariate-normal distributions, underlying many classification algorithms. Using the algorithm, we have classified a 10,000 km<sup>2</sup> area of the BOREAS southern study area. Our classification shows that low-productivity wetland conifer is the dominant land cover and that nearly 7% of the area is occupied by boreal fens, a major source of methane. In addition, nearly 23% of the area has been disturbed by either fire or logging in the last 20 years, suggesting an important role for disturbance to the regional carbon budget. A thorough evaluation of the physically based classifier within the southern study area shows accuracies superior to those obtained with conventional statistically based algorithms, implying even better performance when extended over multiple Landsat frames since the physically based approach can account directly for regional variations in reflectance resulting from varying illumination and viewing conditions (topography, Sun angle). The conifer biomass density estimation algorithm is based on our discovery of a convenient natural relationship between crown height and volumetric density that renders the biomass density for black spruce stands independent of tree height, and a function only of sunlit canopy fraction. This permits us to calculate directly the relationship between reflectance and biomass density. An evaluation of the algorithm using ground sites shows our algorithm can estimate black spruce biomass density with a root-mean-square error of 2.73 kg/m<sup>2</sup> for correctly classified sites. Our evaluation also demonstrates the importance of correct classification. Root-mean-square errors for misclassified sites were 3.96 kg/m<sup>2</sup>. Using this approach we have estimated the biomass density in the BOREAS southern study area for the dominant land cover type in the circumpolar boreal ecosystem, wetland black spruce. These results show a bimodality to the biomass density regional distribution, controlled perhaps by underlying topographic and edaphic factors.

### Introduction

With the launch of Landsat in July 1972 we have been able to periodically observe the Earth's surface for nearly a quarter century. During this same period, considerable investment in intellectual and financial resources has gone into the development of physically based models relating vegetated biophysical

characteristics to the bidirectional reflectance properties of vegetation. Beginning with the work of *Goel and Thompson* [1984], such models have been used to infer surface vegetation characteristics from their reflectance properties. While much progress has been made in this latter regard, no physically based algorithms exist to both classify vegetation and infer its biophysical characteristics.

In part this is a result of a lack of reliable calibration and atmospheric correction techniques, both of which are required for physically based inference of vegetation properties. With-

This paper is not subject to U.S. copyright. Published in 1997 by the American Geophysical Union.

Paper number 97JD02578.

out calibrated, atmospherically corrected satellite data the remote sensing community has had to rely on statistically based techniques, such as supervised or unsupervised classifiers to classify images and empirical regression techniques to relate various vegetation indices to biophysical parameters such as biomass density (BMD), leaf area index (LAI), or the fraction of absorbed photosynthetically active radiation (Fapar). With the advent of the EOS AM1 platform the community will have, for the first time, absolutely calibrated and atmospherically corrected remote sensing data adequate to the task of integrated, physically based classification and biophysical parameter estimation. This paper develops a paradigm for such an approach.

In the background section we will briefly review the status of remote sensing algorithms. In that context we next state the goals and objectives of our current effort as they relate to and are defined by the needs of the global change research program and the state of the art of existing classification, biophysical characteristics inference algorithms.

In Methods, we describe an integrated, physically based classification and biophysical characteristic estimation algorithm that utilizes canopy reflectance models in both classification and biophysical characteristics estimation. The algorithm permits us to account directly for the effects on class signatures and surface reflectance of seasonal growth patterns and variations in illumination and viewing conditions (topography, Sun angle).

Finally, in Results, we discuss the classification and biophysical characteristics estimation maps developed over the BOREAS southern study area [Sellers *et al.*, 1995] which result from our algorithm, and evaluate these products using in situ measurements of community composition and biomass density for eight black spruce (*picea mariana*) and nine jack pine (*pinus banksiana*) sites.

## Background

The mainstays of pattern recognition techniques are the statistically based supervised and unsupervised classification approaches. Supervised classification algorithms are based on statistical maximum likelihood decision theory [Swain and Davis, 1978; Mather, 1987; Townshend *et al.*, 1991]. These algorithms utilize multivariate, multispectral reflectance data and rely on training data to develop decision regions, i.e., associations between land cover classes and data vectors in the multivariate data space. In many applications a parametric form of supervised classification is used in which multivariate Gaussian functions are assumed to represent the statistical distributions of the multispectral data vectors associated with each land cover class. Hall *et al.* [1995] have shown that the Gaussian assumption is clearly not a good representation for many vegetation classes. Furthermore, the misclassification error resulting from the Gaussian assumption can cause large errors in the estimation of LAI and Fpar. Unsupervised classification algorithms cluster the multispectral remote sensing data and ancillary data, such as digital elevation maps, and generate unlabeled cluster maps [Ball and Hall, 1967]. To label the clusters, the cluster maps are compared with field data or maps of known land cover. The problem with the unsupervised approach is that the user must determine the number and size of the clusters with no theory to guide the selection of these parameters. As a result, the multivariate space is partitioned

rather arbitrarily and does not necessarily conform to the actual distributions of measurements associated with each class.

Whether the procedure chosen is supervised, unsupervised, or hybrids of the two, incorrect assumptions regarding the statistical multivariate distributions can actually reduce the inherent spectral distinguishability among classes. This fact is the basis for the common experience that classes are often much more distinct in false color images than in the classification image based on the same bands. The advantage of these purely statistical approaches, whether they be supervised or unsupervised, is that no physical understanding of how multispectral reflectance is related to land cover is required to use them. However, the “signatures” derived from the training sample, i.e., class means and covariances, must be computed from a training sample that is statistically representative of the entire region being classified, a condition difficult to achieve in practice. Nonparametric approaches have been developed to avoid the difficulties inherent in statistical pattern recognition. One such approach is the decision-tree method in which rules are used successively. For example, Lloyd [1990] used a binary decision-tree classifier based on summary indices derived from time series NDVI data. Unless the values of the branching points and thresholds are physically based, such classifiers have limited regional and temporal applicability.

In addition to the “per pixel” classification algorithms, there are a number of classification algorithms that utilize spatial information; that is, they operate on groups of pixels and take advantage of the spatial statistics (e.g., texture) to identify classes; examples are contextual classifiers [Settle, 1989], or image segmentation [Kettig and Landgrebe, 1976]. While these approaches can improve classification accuracy, they still suffer from the reliance on purely statistical relationships.

One of the early attempts to utilize physical understanding of the relationship between vegetation growth patterns and multispectral signatures was to model the time variation of signatures [Badhwar *et al.*, 1982]. This model, based on the logistic model for vegetation growth, recast the classification problem in terms of physically understandable vegetation-specific growth parameters: the seasonal leaf area duration, the characteristic time of “greenup,” the characteristic time of peak greenness, and the peak greenness (or vegetation index) which could be determined from a knowledge of the phenological behavior of different crops, or estimated from a temporal series of reflectance measurements. Hall and Badhwar [1987] were able to determine values for these characteristic parameters for corn and soybeans and developed a labeling logic from training data in the United States. Their work showed that the same labeling logic and signatures could be used to successfully classify corn and soybeans in both the United States and Argentina, thus reducing the dependence on training data.

A somewhat different approach to image classification has its basis in mixture decomposition [Horowitz *et al.*, 1975], a technique that decomposes a pixel into its areal proportions of spectrally distinct land cover elements, for example, shadow, sunlit canopy, and sunlit background. The choice of these elements is driven by the particular application; however, they must be spectrally distinct from each other (so-called “end members”) and their number equal or less than the number of available spectral bands. Mixture decomposition algorithms have been used, for example, to measure the regional abundance of vegetation in deserts [Smith *et al.*, 1990a, b]. Mixture decomposition has also been used for land cover classification

extensively in the humid tropical forests [Novo and Shimabukuro, 1994; Shimabukuro et al., 1994; Shimabukuro and Smith, 1995].

In some respects, mixture decomposition is a linear transformation from spectral space into a “structure” space (e.g., shadow, sunlit canopy, sunlit background). The advantage of such a transformation is that the structure values are more easily understood in terms of land cover type and biophysical parameters than are the multivariate spectral reflectance values directly. Hall et al. [1995] have shown, for example, that LAI and biomass density can be computed directly in terms of shadow fraction and sunlit background using simple geometric shadowing models of conifer canopies.

In all the approaches discussed above, class signatures are affected by seasonal variations in vegetation as well as other factors such as illumination angle, view angle, topography. Thus an algorithm trained at one time of the year or region is not likely to work at a different time of the year or in a different region, which makes the purely statistical or empirical techniques labor intensive and often unreliable over large regions or for multiyear sequences of images.

As will be seen in the description of our physically based approach, we compute directly the multispectral decision regions for a particular set of land cover types, based on radiative transfer theory and utilization and a host of other information available to identify land cover type. Thus we are able to compute directly and utilize the highly nonlinear shape of the  $n$ -dimensional multivariate distributions and account directly for their variation as a function of illumination, view angle, and seasonal differences.

#### Status of Remote Sensing Algorithms for Biocharacteristics Estimation

There are two broad classes of remote sensing algorithms for inferring vegetation biophysical properties: (1) empirical algorithms, which curve-fit vegetation biophysical properties for a particular vegetation type to reflectance and/or vegetation indices, and (2) physically based algorithms, which depend on radiative transfer models to relate surface reflectance to vegetation type and biophysical properties.

While simple to implement, there are a number of problems that limit the ultimate performance of the empirical approaches, the most serious being their inability to deal with variation in environmental conditions, Sun and illumination angle, vegetation understory or background, and variations in the structure and optical characteristics of the vegetation itself.

The fundamental basis for physically based remote sensing algorithms is radiative transfer models that specify the physical relationship between spectral reflectance  $\rho$  and the structure and optical properties of the target [Goel, 1988]. For a vegetated surface, radiative transfer theory can be used to quantify  $\rho$  as a function of the major scattering and absorption elements of the canopy. In theory, quantitative remote sensing is the inference of these properties by “inversion” of  $\rho$  for the target properties, given a set of reflectance measurements from the targets in different spectral regions and at specified view and illumination angles [Goel and Thompson, 1984; Goel and Grier, 1988].

There are a number of practical problems that prevent the straightforward application of this approach at regional or global scales. For vegetated targets, most radiative transfer models (except for coherent scattering models used for active sensors) compute single-canopy reflectance as a function of

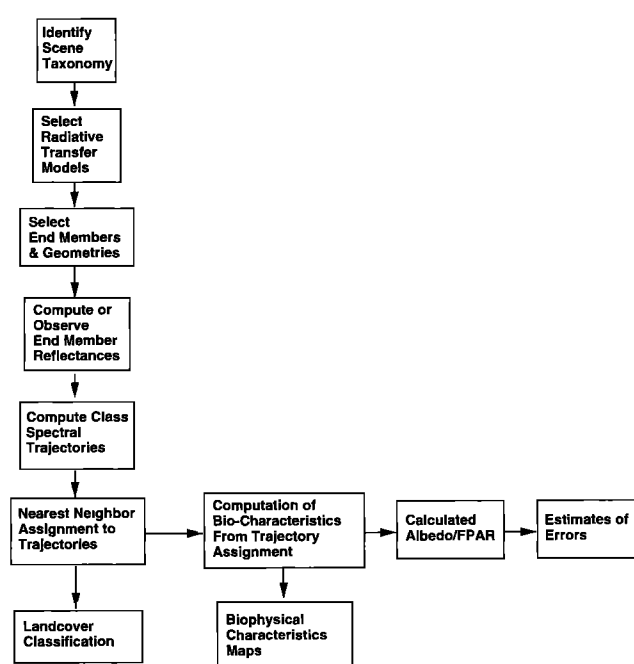


**Figure 1.** Algorithmic flow diagram for physically based classifier and biophysical characteristics estimation algorithm.

canopy leaf and bark optical properties (LOP), leaf area index (LAI), canopy leaf angle distribution (LAD), view and illumination zenith and azimuth ( $\theta$ ,  $\phi$ ), downwelling illumination  $I(\theta, \phi)$  distribution. The reflectance for a landscape element, consisting of multiple canopies depends on even more variables. A landscape element can consist of multiple vegetation types each with different properties, and thus the radiative transfer model must also account for spatial variability in the single-canopy properties as well as variations in canopy spacing, leafy to woody biomass ratios, and in understory (or background) reflectance.

Such complexities raise two very practical problems in the inversion of  $\rho$ : (1) the inversion problem is underdetermined; that is, there are many more unknowns than there are independent measurements; and (2) no single radiative transfer model can successfully represent  $\rho$  for the large range of canopies that can occupy a given pixel in a regional or global landscape.

To circumvent these problems at regional and global scales, we first “stratify” the landscape by land cover type and then apply land cover type-dependent models and algorithms within each stratum. Stratification into land cover type reduces the number of unknowns that must be dealt with and, in addition, specifies which radiative transfer model is required for the inversion.

#### Methods

The algorithm we describe and evaluate is an integrated sequence of operations (Figure 1) which uses physically based canopy reflectance models to both classify satellite image pixels and estimate the biophysical parameters of the vegetated land cover. The physical canopy reflectance models are specific to each land cover type. Although the technique can be expanded to include multitemporal, multiangle data, we used only peak

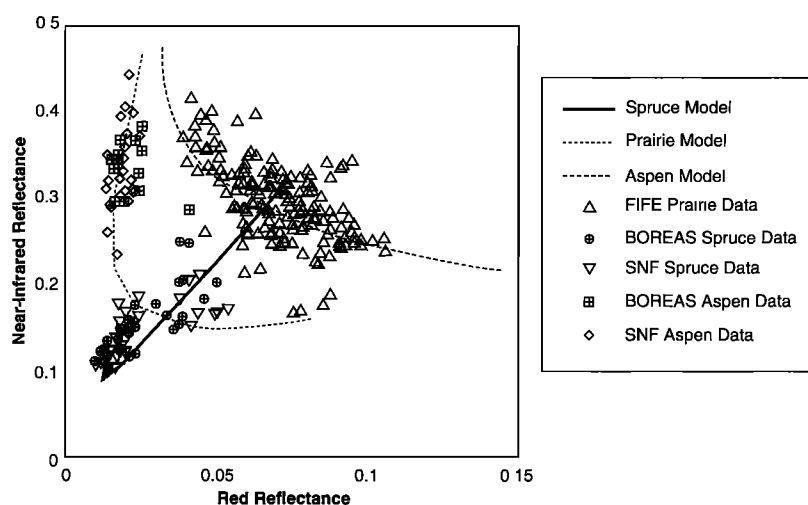


**Figure 2.** Red and near-infrared canopy reflectance model trajectories (solid lines) for aspen (*Populus Tremuloides*), black spruce (*picea mariana*), and FIFE prairie grasses as compared to field-measured values of black spruce and aspen reflectance measured during 1983 and 1984 from the COVER project [Hall et al., 1992] and during 1994 during the BOREAS project [Sellers et al., 1992]. Prairie grass measured values were acquired in 1987 and 1989 during the FIFE project [Sellers et al., 1988, 1992]. Aspen and black spruce reflectances were modeled using the GeoSail model [Huemmrich, 1997]; prairie reflectance was modeled by using the SAIL model [Verhoef, 1984].

growing season, near-nadir satellite data for the initial development.

Canopy reflectance models are used in the classification algorithm to define spectral reflectance trajectories for each land cover class. Positions along each trajectory correspond to unique areal canopy cover fractions ranging from zero to unity. To classify a multispectral value, it is assigned to the “nearest” multispectral trajectory using a simple Euclidian distance metric. This nearest-neighbor rule defines decision regions in the multispectral space for each land cover class.

In Figure 2 the reflectance predictions from such geometric models (lines) as well as field measurements (plot symbols) are plotted for three diverse land cover types. Each trajectory begins at a red-near-infrared (NIR) reflectance value of the background peculiar to that class, i.e., when the canopy cover fraction for that class is zero. The trajectory ends at the red-NIR reflectance point of the class when its canopy cover is unity. As can be seen, the different vegetation types have quite different red-NIR reflectance trajectories. The hook-shaped trajectory of black spruce results from the fact that as sunlit canopy fraction increases, shadow fraction increases and sunlit background fraction decreases (the sum of this triplet is unity) until the sunlit crowns become sufficiently dense to obscure illuminated background. At this point, which we call the critical density, shadow fraction begins to decrease. For black spruce the use of a multivariate Gaussian function to model the statistical distribution of reflectance values would clearly be inappropriate.

The reflectance model predictions are compared in Figure 2 to canopy reflectance data measured over these land cover types for three different test sites, over a 10 year span, in three different regions: (1) spectral reflectance data taken during 1983 and 1984 over black spruce sites in the Superior National Forest in the northern part of Minnesota [Hall et al., 1992], (2) data taken during the FIFE experiment in Kansas during 1987 and 1989 [Sellers et al., 1988, 1992; Strebel et al., 1994], and (3) data taken over black spruce sites in central Canada in 1994

during the BOREAS experiment [Loechel et al., this issue]. The comparisons demonstrate that at nadir view, with atmospherically corrected, calibrated reflectance data, canopy reflectance can be represented over a wide range of years and regions using reasonably simple canopy reflectance models. The models provide a reasonably accurate description of the directional reflectance of a diverse array of land cover types indicating that the macroscale structure of a land cover type is a key factor in determining reflectance.

Using these canopy reflectance models permits us to compute land cover signatures as a function of factors that can vary widely from one acquisition date to the next, or from one region to the next: background reflectance, phenology, canopy cover, solar illumination angle, and topographic variations. Computing signatures from physically based canopy reflectance models results in a much more robust signature extension over large regions and over time than conventional statistical training, or even neural net training methods. For example, as shown in Figure 3, aspen red-NIR reflectance will depend strongly on solar zenith angle. Because we know the solar illumination angle for each acquisition, we compute customized signatures for each acquisition date and each cover fraction. This alleviates the problems encountered with neural net or statistical techniques, for example, applying empirical solar illumination angle corrections that apply to all cover types in a scene, regardless of their biomass density, for example, as is the case for the FASIR algorithm [Sellers et al., 1994].

#### Computation of $n$ -Space Spectral Reflectance Trajectories

The canopy reflectance models used for this study are hybrids of geometric models [Jasinski and Eagleson, 1990; Huemmrich, 1997] and the SAIL model [Verhoef, 1984] with geometric and optical property parameters adjusted to each land cover type. Geometrical models are most useful for shadow-dominated canopies such as shrubs, open forests, orchards, and early stages of crop growth where shadowing dominates multiple scattering. Model parameters are developed from (1)

**Table 1.** Reflectance Values for End Members Used to Derive Spectral Reflectance Trajectories for Physically Based Classification

	Wet Conifer		Dry Conifer		Deciduous	
	Red	NIR	Red	NIR	Red	NIR
$\rho_b$	0.0456	0.1873	0.234	0.394	0.083	0.16
$\rho_c$	0.0465	0.3033	0.0702	0.3735	0.0512	0.4099
$\rho_{sr}$	0.0004	0.0137	0.0011	0.0162	0.00046	0.0207

prior knowledge of the canopy optical and background properties of the land cover classes in a stratum or (2) estimates of background and canopy reflectance properties using limited amounts of satellite training pixels. In the subsections to follow we will describe each of the above steps in additional detail.

Using such models, pixel-level reflectance  $\rho_i$  in any band may be computed as a function of (1) the pixel fraction and reflectance of “end members,” for example, sunlit canopy, sunlit background, and shaded background, and (2) view and solar illumination angle. Using this approach, a land cover type is described as a number of geometrical shapes placed on a background surface. It is assumed that each satellite sensor pixel views collections of individual trees. Pixel-level reflectance can thus be computed as a linear mixture of sunlit tree tops, sunlit background (or understory), and shadows. To develop a closed-form mathematical expression for this observed dependence of red-NIR reflectance on canopy biophysical characteristics, the reflectance of each component in the scene is weighted by their fractional area and summed:

$$\rho_i = C\rho_c + S\rho_s + B\rho_b \quad (1)$$

where

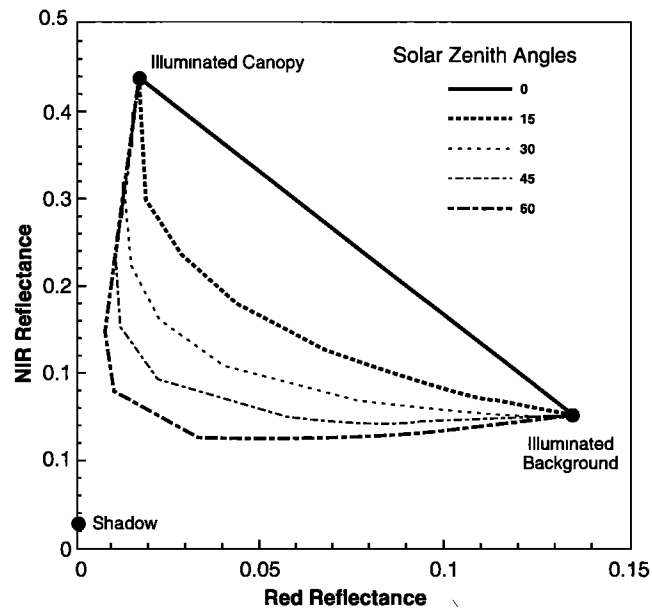


**Figure 3.** Dependence of red-NIR reflectance on solar zenith angle (from vertical) as computed from the hybrid canopy reflectance models. Note the widely divergent nature of the dependence on canopy cover and land cover classes which would render a single correction ineffective and thus signature extension difficult with nonphysically based classification algorithms.

$\rho_i$  = pixel-level reflectance;  
 $\rho_c$  = canopy reflectance;  
 $\rho_s$  = shadow reflectance;  
 $\rho_b$  = background reflectance;  
 $C$  = sunlit canopy fraction;  
 $S$  = fraction of shadow (canopy plus background);  
 $B$  = fraction of sunlit background.

To calculate  $S$  as a function of  $C$ , canopies are assumed to be geometric forms randomly distributed on a horizontal plane. For a nadir view angle, shadow fraction

$$S = 1 - C - (1 - C)^{(\eta+1)} \quad (2)$$

and the background fraction  $B$  is given by

$$B = 1 - C - S. \quad (3)$$

Canopy shapes can be spheres, ellipsoids, cones, or cylinders or portions or combinations of these forms. The shapes, dimensions, number, and placement of the canopy forms are defined in the model, as are the optical properties of the background and canopy. The  $\eta$  is the ratio of shadow area to canopy area for a single tree and is a function of a single parameter  $b$  (the ratio of the canopy's characteristic height to its width or diameter) and the solar zenith angle. For example, for cylinders,  $\eta$  is given by  $4/\pi (\tan \theta/b)$ , where  $\theta$  is the solar zenith angle, or for cones,  $\eta$  is  $(\cot \varphi - \pi/2 + \varphi)/\pi$ , where  $\varphi$  is  $\tan^{-1}(b)$ . Thus a number of different crown shapes can be represented rather simply, and the only parameter that must be estimated is a characteristic height to width for the crown. Thus conifer trees might be represented by the cone and deciduous trees by an ellipsoid. Characteristic dimensions for many of these canopies are available from the allometric literature and, in some cases, have been estimated directly using reflectance model inversion.

#### Determination of End Member Reflectances

To estimate the end member reflectances  $\rho_s$ ,  $\rho_b$ , and  $\rho_c$  in (1), we used a combination of ground-observed and satellite-observed reflectances of scene end member samples as well as canopy reflectance model calculations. The resulting reflectance values are shown in Table 1. Estimation of end member reflectances amounts to training the physically based classifier; however, far fewer samples are required than for a Gaussian maximum likelihood or neural net algorithm. Since only end member reflectances are being estimated, the training sample does not have to meet the more stringent requirement of being statistically representative as with the more empirical approaches.

For the wet conifer class, predominately black spruce, tree density is strongly related to water table depth. Thus we chose open fen where no overstory is present as the background end

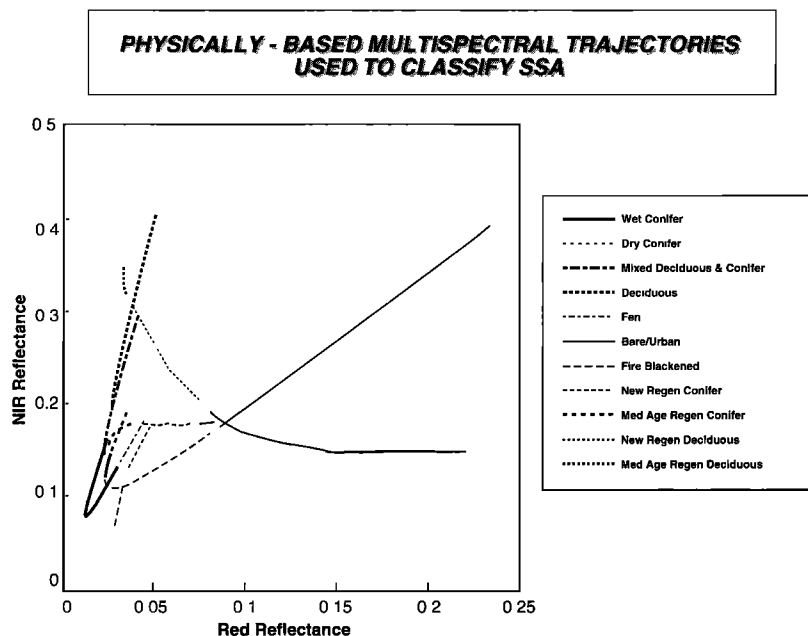


**Figure 4.** Final spectral trajectories used in the physically based classification and biophysical parameter estimation algorithm.

member. Open fen results when the water table rises to the surface, prohibiting the development of trees. Open fen reflectance  $\rho_b$  was measured by identifying open fen areas from air photos, then finding the corresponding groups of pixels in the TM imagery. To avoid water contamination, those pixels with the highest reflectance were selected. As an alternative, ground-measured values of open fen reflectance could also be used.

For wetland conifer-shadowed background reflectance  $\rho_c$  we used ground measurements of sphagnum moss reflectance, a common background species in conifer wetlands, and the SAIL model to compute the reflectance of shadowed sphagnum moss. The SAIL model was used to compute the transmittance of black spruce canopies. We used the ratio of downwelling direct and diffuse illumination to the background-reflected shadowed illumination as our estimate of shadowed reflectance. Conifer trees were represented by cones. When solar zenith angles exceed the cone apex angle, the cone will be partially self-shaded. In our model implementation we assumed that the shaded tree and shadowed background reflectance were equal.

For the wet conifer sunlit canopy end member we solved (1) for  $\rho_c$ , using the values for  $\rho_c$  and  $\rho_b$  as determined above, and the geometric canopy reflectance model to compute the maximum shadow fraction  $S_{\max}$  (and the corresponding values of  $C$  and  $B$ ) at which the minimum wetland conifer reflectance  $\rho_{\min}$  for each spectral band occurs. Then we used the lowest reflectance wetland conifer TM pixels in the scene to estimate  $\rho_{\min}$  for each band. These values then permitted us to solve (1) for  $\rho_c$ .

For dry conifer-shadowed background reflectance  $\rho_c$  we used ground measurements of lichen reflectance, a common background species in jack pine stands, and the SAIL model to compute the reflectance of shadowed lichen. As with wetland conifer, we used the ratio of downwelling direct and diffuse illumination to the lichen-reflected shadowed illumination as our estimate of shadowed reflectance.

For the deciduous trajectory we used cylinders as the geometric form and ground-measured reflectance for the sunlit aspen canopy and leaf litter. The shadow reflectance was calculated by using the SAIL model as with wetland conifer.

A trajectory for mixed deciduous/conifer as a function of canopy cover was computed by a weighted average of the two conifer trajectories and the deciduous trajectory. Because no mid-infrared (MIR) end member reflectances or optical properties were available to us we estimated the third MIR dimension of the spectral trajectory for each class by selecting “training” pixels of each cover class then utilizing the reflectance triples (red, NIR, MIR) from these samples to empirically establish the spectral trajectory’s third MIR dimension.

For the regeneration classes, we did not have the allometry data available to characterize the geometric structure of the canopies as a function of successional stage. For these classes, multispectral trajectories were fit through reflectance values for training pixels. Figure 4 shows the final spectral trajectories resulting from the above procedures.

#### Land Cover Classification and Biomass Density Estimation

Each pixel is classified by land cover type according to the multispectral trajectory which it is “closest” to in a nearest-neighbor sense. To implement this numerically, we used the theoretical and empirical methods described in Methods to compute tables of multispectral values for each of the class spectral trajectory as a function of its end member fractions and reflectances. The Euclidian spectral distance of each image pixel to each multispectral value in the table was then computed and the minimum value used to define which class trajectory the pixel was “closest” to. A more formal classification strategy can be developed by using statistical optimization theory. Such optimization theory could be employed to minimize biophysical characteristic estimation error resulting from misclassification error.

Given the classification assignment for a pixel and its nearest-neighbor multispectral value from the table, the associated

end-member values are implied and thus biomass density for the pixel can be computed from the end member fractions and their relationship to crown volume. As we now show, allometric relations relating crown volume to crown biomass can be used to related biomass density to the end member fractions. The canopy biomass density (BMD), biomass per unit of horizontal surface area, is by definition the product of  $\nu_b$ , its volumetric mass density (kilogram of biomass per cubic meter of crown), and  $\nu_v$ , its crown volume density ( $\text{m}^3$  of crown per  $\text{m}^2$  of ground area). That is,

$$\text{BMD} = \nu_b \nu_v \quad (4)$$

For nadir viewing sensors and a conical-shaped crown,  $\nu_v$  is given by

$$\nu_v = (C_t/3)h \quad (5)$$

where  $C_t$  is the total (sunlit plus shadowed) canopy fraction, and  $h$  is the average canopy height; Thus BMD can be computed by

$$\text{BMD} = \nu_b(C/3f)h \quad (6)$$

where  $f$  is the ratio of the sunlit canopy fraction  $C$  to the total  $C_t$ .

In general, to use (6) for BMD, we must not only estimate  $C$  from mixture decomposition but we must also estimate  $h$ . Tree height is difficult if not impossible to estimate from passive optical remote sensing data; however, we show in the Appendix that  $\nu_b$  must be inversely related to  $h$  when crown morphology satisfies two conditions, namely, that (1) crown base diameter is proportional to the bole diameter at breast height and (2) tree biomass is proportional to the square of the diameter at breast height.

For black spruce the allometric data taken from the COVER experiment in Minnesota [Hall et al., 1992] and from the BOREAS experiment show conditions to be approximately satisfied, and from the Appendix the relation between  $C$  and BMD in (6) is given more precisely by

$$\begin{aligned} \text{BMD} &= 34.4 C \text{ (kg/m}^2\text{)} - \text{Superior National Forest} \\ \text{BMD} &= 31.4 C \text{ (kg/m}^2\text{)} - \text{BOREAS} \end{aligned} \quad (7)$$

In effect, conditions 1 and 2 imply an inverse biophysical relationship between  $\nu_b$  and  $h$ , causing  $h$  to cancel in (6); this makes possible the use of optical data to estimate BMD without direct knowledge of tree height, an important result since tree height is difficult to obtain from passive remote sensing. The inverse relation between  $\nu_b$  and  $h$  in physical terms means simply that smaller trees on average are more dense trees volumetrically.

As an independent confirmation of this relationship, we used TM satellite data acquired from eight black spruce sites in the BOREAS study area to estimate  $C$  from the spectral trajectory model and compared  $C$  to the ground-observed biomass densities for those sites. The result is shown in Figure 5. The slope of this plot yields a biomass coefficient of 28.8. The approximate agreement between these three independently computed values suggests a reasonably robust relationship between  $C$  and BMD over years and between regions.

When allometric data are not available, an alternative to compute the relationship between BMD and  $C$  is to utilize the satellite data directly given an approximate knowledge of the maximum biomass density expected for each land cover class.

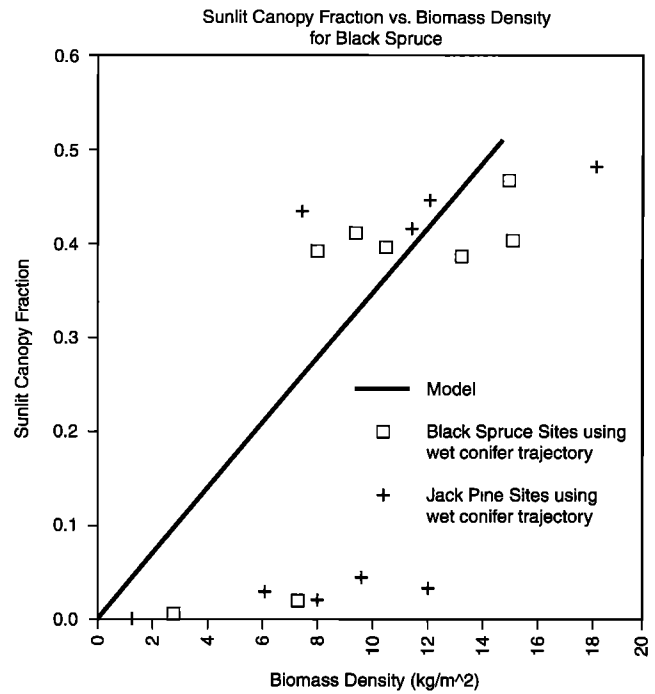


**Figure 5.** Plot of sunlit canopy fraction as estimated from TM data versus biomass density ( $\text{kg/m}^2$ ) for eight black spruce sites in the BOREAS study area.

In this case we can use the maximum values for  $C$  estimated from the satellite data for that cover class and estimate the linear coefficient by inverting equation (A3) for the constant  $k/f$ ; that is,

$$(k/f) = (\pi/4) \text{BMD}_{\text{max}}/C_{\text{max}} \quad (8)$$

### Evaluation

In evaluating the performance of the algorithm, we estimated both the classification and the biophysical parameter estimation error. Classification error is straightforwardly estimated by comparing the classification map to pixels of known identity. Biophysical estimation error can be estimated by comparing model estimates to ground estimates for both correctly and incorrectly classified pixels. When the biomass estimation algorithm is applied to a pixel with an incorrect identity, for example, applying the wet conifer algorithm to a deciduous pixel, large errors can result. To estimate the overall error we had to consider a joint error model between the physically based classifier and the physically based biomass estimator.

**Classification error.** To evaluate the classifier, we compared classification results to ground-identified sites in both the BOREAS southern and northern study areas. A  $3 \times 3$  pixel window was the basic unit of classification; classification errors were computed from frequencies of agreement and disagreement between the classified TM product and the ground-identified sites. The contingency matrices shown in Table 3 were used to quantify between class and within class performance. The rate or frequency of commission of land cover class  $\omega_i$  with land cover class  $\omega_j$  is the frequency with which pixels in class  $\omega_i$  were mistakenly assigned to class  $\omega_j$ . That is,

$$E_{ij} = n(\omega_i > \omega_j)/n(\omega_i) \quad (9)$$



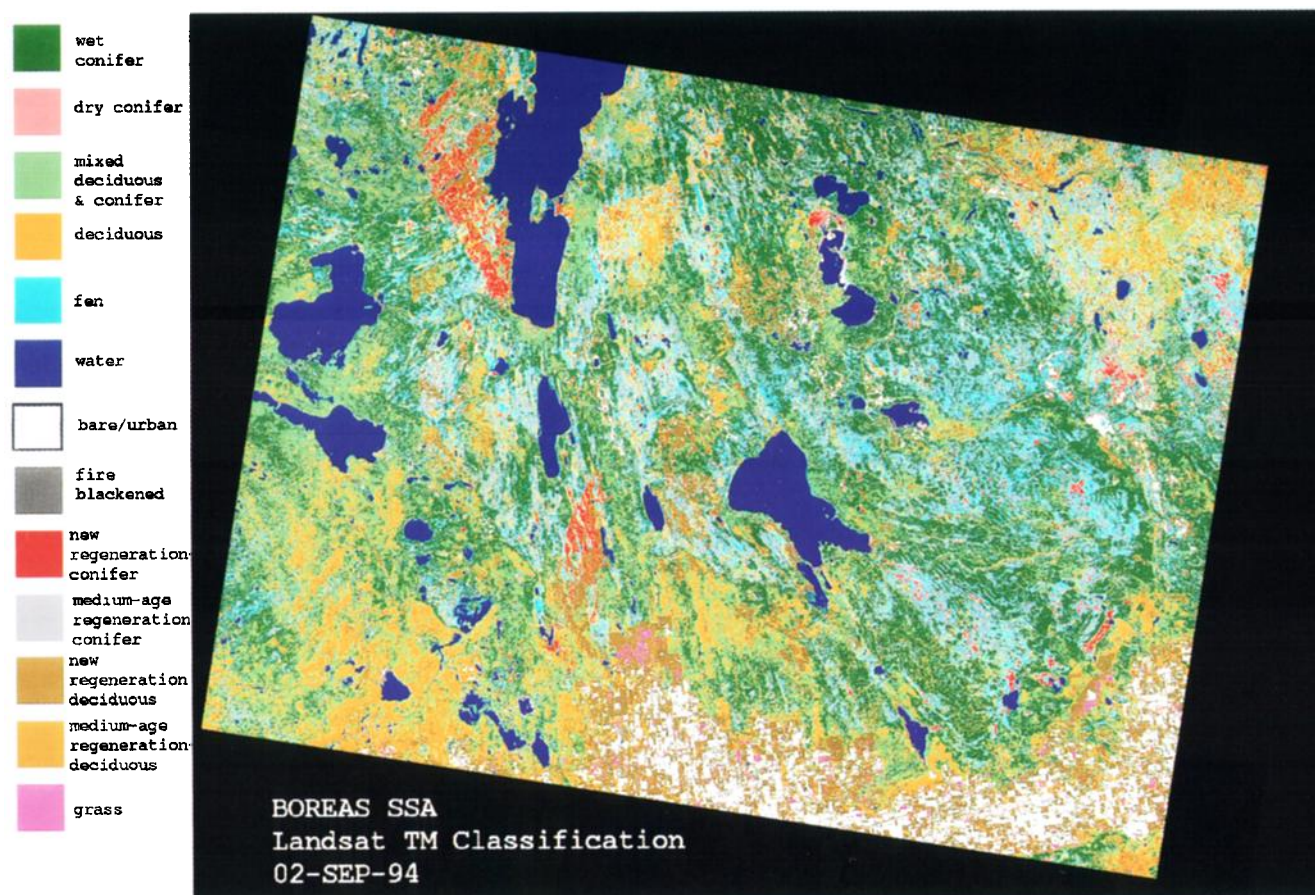


**Plate 1.** Physically based classification of a September 1994 TM image of the BOREAS southern study area (SSA).

The rate or frequency of agreement for class  $\omega_i$  is the frequency with which land cover class  $\omega_i$  was correctly classified as class  $\omega_i$ .

$$P_{ii} = n(\omega_i > \omega_i) / n(\omega_i) \quad (10)$$

The rate or frequency of omission of land cover class  $i$  with any other class is given as

$$E_{ii} = [n(\omega_i) - n(\omega_i > \omega_i)] / n(\omega_i) = 1 - P_{ii} \quad (11)$$

where  $n(\omega_i > \omega_j)$  = number of test pixels in land cover class  $i$  classified as land cover class  $j$ , and  $n(\omega_i > \omega_i)$  = number of test pixels in land cover class  $\omega_i$  classified as land cover class  $\omega_i$ .

With these counts of correct and incorrect classification of test pixels, error rates or frequencies were estimated. To display all types of frequencies discussed above, the classification “agreement” or “contingency” matrix  $C$  of Table 3 was used. The diagonals of  $C$  are frequencies of agreement; the off diagonals are commission frequencies. We chose the rows of the contingency matrix as the “true” labels of the test pixels and the columns to represent the labels assigned to the test pixels by the classifier. The  $i$ th row and  $j$ th column of the matrix is  $E_{ij}$  and the diagonals are  $P_{ii}$ .

**Biomass density estimation error.** In order to compute the regional BMD estimation error, one must account for both correctly and incorrectly classified pixels. Relations between biomass density and canopy cover fraction differ among classes, thus applying such relations to an incorrectly classified pixel can result in large biomass estimation error. To estimate

biophysical estimation error when wet conifer pixels were correctly classified, we again used ground measurements and compared them to our satellite-based estimates. The set of measurements came from BOREAS auxiliary sites, chosen to be homogeneous over at least a 100 m square area for TM comparisons. The regional BMD estimation error, including incorrectly classified pixels, is in essence the weighted average of the mean square biomass estimation error  $e_{ww}$  for correctly classified pixels and the mean square biomass estimation error  $e_{wj}$  when applying the biomass estimator for class  $w$  to pixels from the  $j$ th class incorrectly classified as class  $w$ .

**Table 2.** Estimated Areal Proportions of Carbon/Water/Energy Classes Occupying the SSA

Land Cover Type	Percent of SSA
Wet conifer	27.4
Dry conifer	1.0
Mixed/deciduous and conifer	15.4
Deciduous	13.5
Fen	6.9
Water	8.5
Bare/urban	4.0
Fire blackened	0.0
New regeneration conifer	2.4
Medium-age regeneration conifer	10.2
New regeneration deciduous	9.3
Medium-age regeneration deciduous	0.8
Grass	0.6



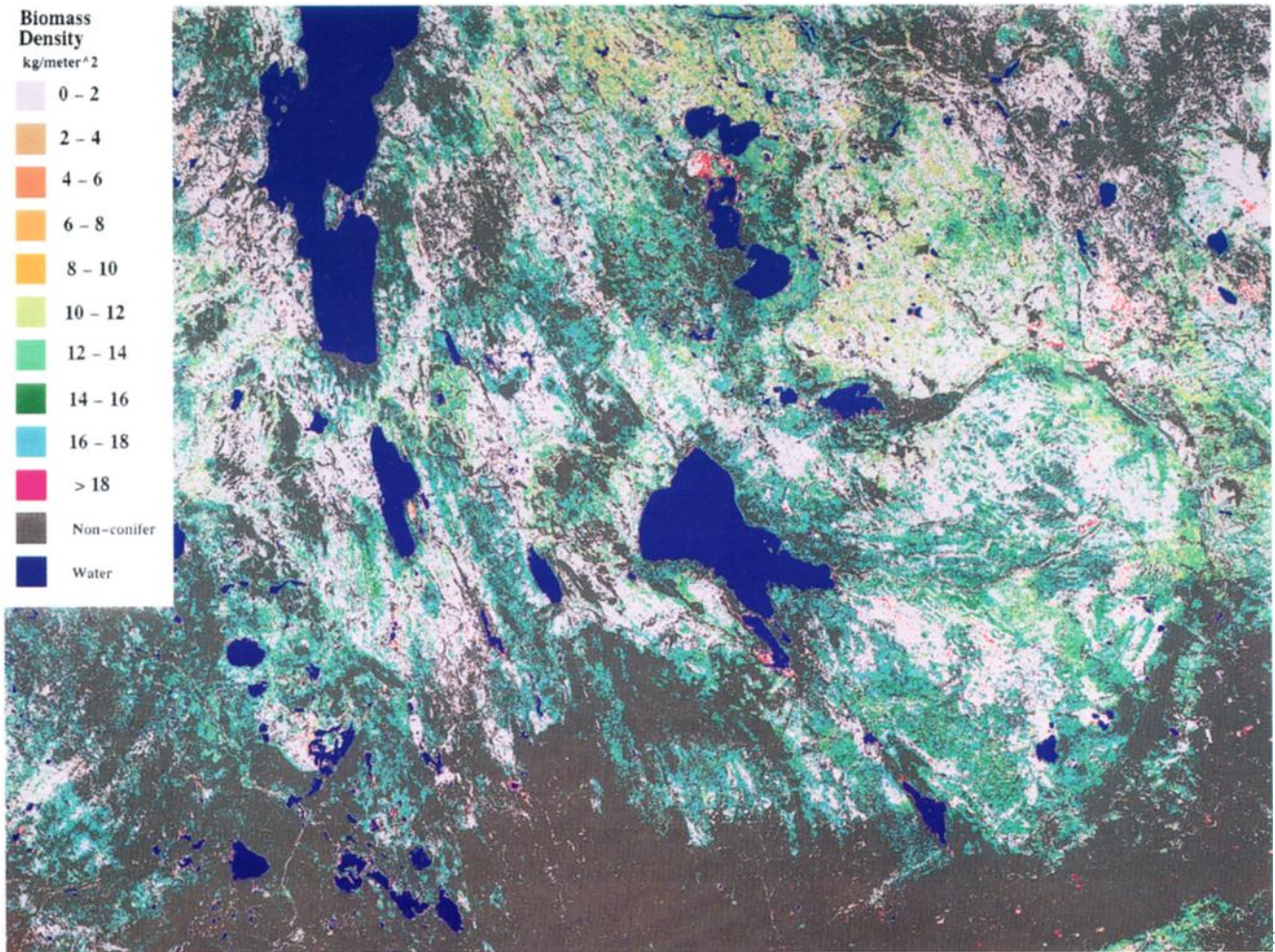


**Plate 2.** Physically based biomass density map of wetland conifer land cover corresponding to the physically based classification of Plate 1.

$$\varepsilon_{ww} = P_w P_{ww} e_{ww} + \sum_j P_j E_{jw} e_{wj} \quad (12)$$

The fraction of correctly classified pixels of wetland conifer is  $P_w P_{ww}$ , where  $P_w$  is the fraction of scene pixels classified as

wetland conifer pixels and  $P_{ww}$  is the probability of correct classification for conifer given by (10). The fraction of pixels from class  $j$  incorrectly classified as class  $w$  is  $P_j E_{jw}$ , and the root-mean-square error for that particular confusion event is

**Table 3.** Contingency Matrices for Physically Based SSA Classification As Computed by Comparison of the Classification Map of Plate 1 with  $3 \times 3$  Groups of Pixels Centered Over Ground-Identified Auxiliary Sites

	Classified													$\Sigma$
	Wet Conifer	Dry Conifer	Mixed	Deciduous	Fen	Water	Bare/Urban	Fire Blackened	New Regen Conifer	Med-Age Regen Conifer	New Regen Decid	Med-Age Regen Decid	Grass	
Observed														
wet conifer	0.710	0.006	0.037	0	0.204	0	0	0	0.006	0.037	0	0	0	1
dry conifer	0.278	0.500	0.056	0	0.111	0	0	0	0.056	0	0	0	0	1
mixed	0.361	0	0.528	0.111	0	0	0	0	0	0	0	0	0	1
deciduous	0	0	0.075	0.887	0	0	0	0	0	0	0	0.038	0	1
fen	0	0.014	0.014	0.014	0.583	0	0	0	0.056	0.319	0	0	0	1
water	0	0	0	0	0	1	0	0	0	0	0	0	0	1
bare/urban	0	0	0	0	0	0	0.889	0	0	0	0.111	0	0	1
fire blackened	0	0.111	0	0	0	0	0	0.833	0.056	0	0	0	0	1
new regen conifer	0.111	0	0	0	0.111	0	0	0	0.778	0	0	0	0	1
med-age regen conifer	0	0	0.333	0	0.222	0	0	0	0	0.444	0	0	0	1
new regen decid	0	0	0	0	0	0	0	0	0	0	1	0	0	1
med-age regen decid	...	...	...	...	...	...	...	...	...	...	...	...	...	...
grass	0.111	0	0.222	0	0	0	0	0	0	0	0	0	0.67	1

Regen, regenerating; Med-Age, medium age; Decid, deciduous.



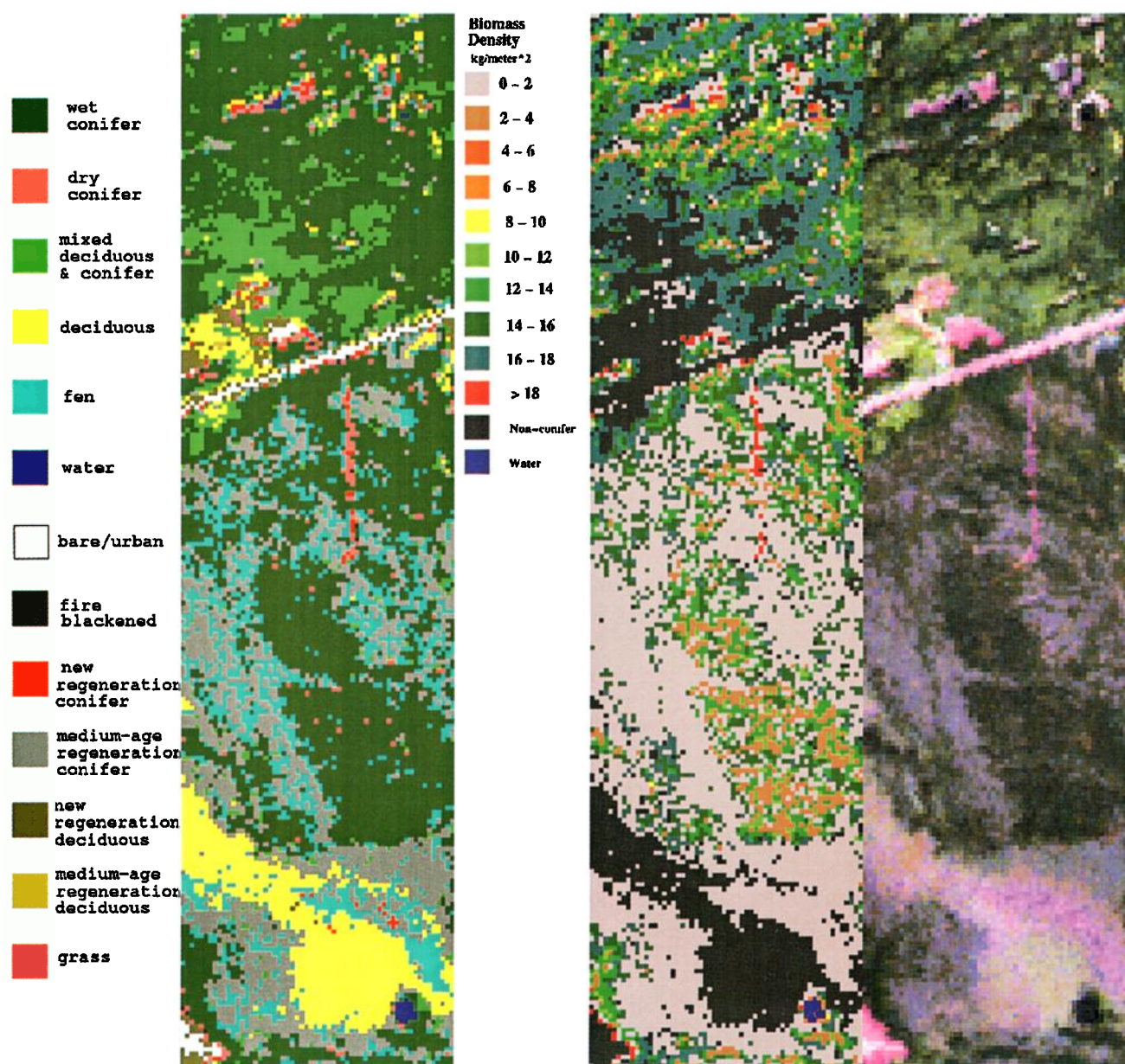


**Plate 3.** (a) Classification image, (b) BMD image, (c) color MIR image of an  $\sim 2 \times 7$  km area in the BOREAS SSA, including the old black spruce tower site.

$P_j E_{jw} e_{wj}$ , where  $e_{wj}$  is the average root-mean-square error when mistakenly applying the biomass estimator for class  $w$  to class  $j$ . Since we did not have ground-observed sites for all classes, we estimated the second term in (12) from the auxiliary sites that were misclassified as wetland conifer.

## Results

Plate 1 is the physically based classification map of the BOREAS SSA. Table 2 displays the estimated areal proportions of each class used in carbon/water/energy modeling. The bright yellow class, deciduous broadleaf, consists primarily of mature aspen and is present in quantities only in the bottom left-hand corner of the scene. The aspen-dominated area is in the Prince Albert National Park where such stands have been protected from logging and fire. In many other areas in the

south, such stands have been logged or converted to croplands, which are classified as bare/urban in this September 2, 1994, image. Otherwise, aspen appears only in mottled late successional patches in the scene, such as in the massive 1977 Fish Lake burn area in the top right-hand corner. In the short term during regeneration through middle age, deciduous broadleaf stands are a strong carbon sink [Black *et al.*, 1996]. However, over a period of multiple fire-regrowth cycles these stands do not appear to be a long-term sink since the carbon stored above ground is released back to the atmosphere by fire.

Large areas of the landscape are dominated by early successional black spruce (red) and regenerating aspen (mustard and darker yellow) following fire. In spite of intense fire suppression in the southern study area (SSA), nearly 23% of the area is in various adolescent stages emphasizing the role of fire in

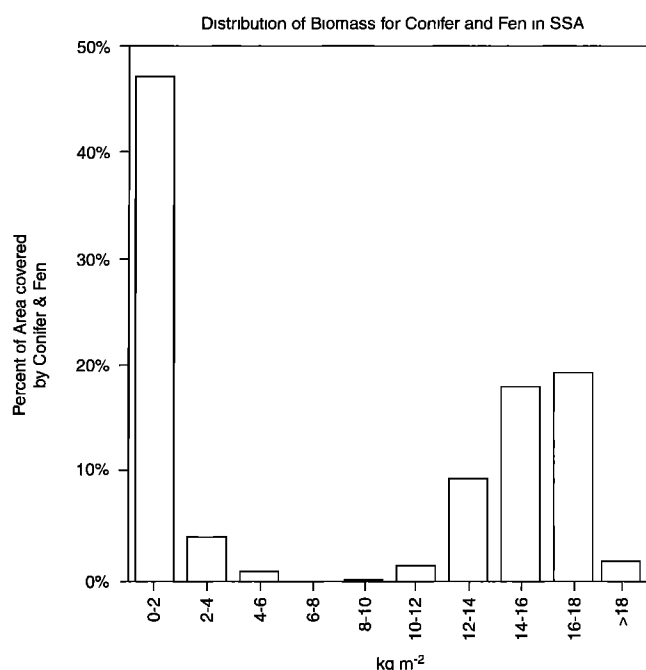


**Figure 6.** Bimodal distribution of BMD values over the BOREAS SSA. The 0–6 kg m<sup>-2</sup> values correspond to sparsely treed fens on peat, whereas the 10–18 kg m<sup>-2</sup> values correspond primarily to black spruce growing on shallow to deep mineral soils.

determining the composition, carbon, water, and energy balance over the boreal forest. *Steyaert et al.* [this issue] analyze AVHRR images and conclude that nearly 30% of the BOREAS study region has been burned within the last 25 years. Annual carbon flux from regenerating stands was not measured during BOREAS, so no direct estimate of their carbon sink strength is available.

In the central and eastern portions of the SSA can be seen a large area of conifer wetlands, including black spruce and tamarack communities (dark green) interlaced with treeless fens (aqua). Such stands dominate the BOREAS SSA and the BOREAS study region in general [*Steyaert et al.*, this issue]. Carbon flux model simulations for the years 1968–1989 [*Frolking et al.*, 1996] show that the extensive conifer wetlands play an important role in the interannual dynamics of global carbon flux. His model simulations predict a loss of 50 g C m<sup>-2</sup> yr<sup>-1</sup> in years with late springs and warm summers, to a gain of –140 g C m<sup>-2</sup> yr<sup>-1</sup> in years with early springs and cool summers.

Clearly, an accurate knowledge of the areal extent of the different boreal forest classes is essential in estimating the strength and interannual variation of the boreal ecosystem as a carbon sink or source. How accurate is our classification product? Our evaluation of (9) and (10) using test pixels in the SSA and the northern study (NSA) resulted in the values displayed in the contingency matrix in Table 3. In this table the diagonals of the contingency matrix are the values obtained from (10) and the off diagonals the values obtained from (9). These values are similar to those reported when applying more traditional classification algorithms to TM or MSS data for boreal forest species [*Hall et al.*, 1991]. The most accurately classified land covers are deciduous, wetland conifer, and the disturbance classes. Wetland conifer is frequently confused with the fen class, a result of the arbitrary canopy cover density bound-

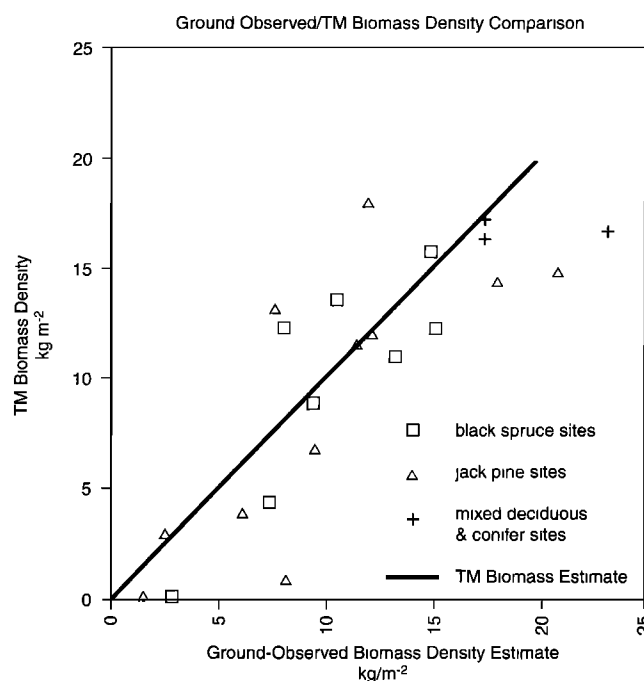


**Figure 7.** BMD estimates from TM for pixels classified by our algorithm as wetland conifer compared to ground-acquired measurements of BMD from plots identified as pure black spruce and jack pine from ground. The root-mean-square error for the correctly classified pixels (black spruce) is 2.75 kg m<sup>-2</sup>; for the jack pine pixels, incorrectly classified as black spruce, the root-mean-square error is 3.99 kg m<sup>-2</sup>; for the mixed sites, incorrectly classified as wet conifer, the root-mean-square error is 3.92 kg m<sup>-2</sup>. The overall root-mean-square error is 3.96 kg m<sup>-2</sup>.

ary of 1/7 selected as the demarcation along the wetland conifer trajectory between untreed fen and treed fen (Figure 4). Even though dry conifer should be spectrally distinct, jack pine with a lichen background, it is confused half the time with either wetland conifer or fen. Why this is so is not completely understood. Fortunately, as can be seen from Plate 1 and Table 2, dry conifer occurs very infrequently and thus plays an insignificant role in the regional-scale energy/water/carbon flux. The mixed coniferous/deciduous class is understandably confused with both wetland conifer and deciduous, a result of the spectral similarities induced by our definition of the mixed class (a patch with <80% of either conifer or deciduous). Thus the wetland conifer class can be very similar spectrally to a mixed conifer/deciduous class. Fen and young to medium-age regenerating conifer are also confused because young and medium-age regenerating wetland conifer has low canopy density and usually regenerates on a moss substrate, spectrally similar to sparsely treed fens.

The color-coded BMD map of the SSA boreal conifers produced by our physically based algorithm is shown in Plate 2. We have chosen a display bin-size of 2 kg m<sup>-2</sup> corresponding approximately to the estimated mean-square-error of the BMD (see next paragraph). The landscape dominated by the light gray color with wave-like patterns of green hues is an extensive conifer wetlands. The blue-green pixels correspond to more productive upland conifer growing primarily on mineral soils. The yellow pixels, widely scattered throughout the scene, correspond to boundaries between treed and untreed

fens in the wetlands. To the south along the bottom of the image, colored dark gray, are the aspen-dominated and upland agricultural areas.

Inspection of this image and the magnified image in Plate 3 reveals a number of vegetation-soil associations typical of the boreal ecosystem. Plate 3 displays in detail correspondences among the false color mid-infrared image, the classification map, and the BMD map over a  $1.8 \times 6.96$  km area in the central portion of the SSA, including the old black spruce tower site. The spatial patterns in the BMD map correspond closely to conifer density variations induced by topographic and edaphic variations in the SSA, known controls on boreal conifer productivity. The light gray areas for the most part are sparsely treed fens where the water table is at the surface producing sparsely treed patches. The green hues correspond to waves of small, more heavily treed, peat and mineral soil mounds slightly above the water table, rendering trees more productive.

One curious result is the bimodal distribution of BMD values shown in Figure 6. The lower mode corresponds to the sparsely treed waterlogged areas, the upper mode to more densely treed peat and mineral soil mounds. The cause of the empty BMD bins from 6 to  $10 \text{ kg m}^{-2}$  is uncertain but is perhaps a result of the rapidly undulating peat mounds commonly observed in patterned fens [Larsen, 1980].

While the qualitative analysis above gives us confidence that the BMD algorithm is producing reliable information, we conducted an analysis to quantify its reliability. In this analysis we compared the TM BMD estimates to a set of ground-acquired data, the BOREAS auxiliary sites, yielding an estimate of the mean square biomass estimation error  $e_{ww}$  in (12) of  $2.73 \text{ kg m}^{-2}$  (see Figure 7). By way of comparison, Hall et al. [1995] used the same GeoSail model employed here to estimate a number of biophysical parameters using helicopter-acquired MMR (TM bands) data acquired over the Superior National Forest during 1983 and 1984 [Hall et al., 1996] obtaining an accuracy  $2.0 \text{ kg m}^{-2}$ . Hall et al. [1996] used a conical model with sunlit canopy reflectance as a function of solar zenith angle and reported improved accuracies of  $1.7 \text{ kg m}^{-2}$  over the same Superior National Forest sites.

Several of the pure jack pine sites, which were not predominantly black spruce, were misclassified as wetland conifer by our algorithm. The algorithm estimates BMD for these pixels on the basis of the black spruce model; thus when the pixel is nonconifer, the error in the estimate can be quite high, as shown in Figure 7. The root-mean-square error for the misclassified pixels is  $3.96 \text{ kg m}^{-2}$  with an overall root-mean-square error of  $3.75 \text{ kg m}^{-2}$ . Thus in regions of spectral space where classification error is predicted from the reflectance models to be large, confidence weights should be assigned so that such points are properly discounted in BMD averaging to the regional scale.

## Conclusions

We have developed and evaluated an integrated, physically based classification and biophysical characteristics estimation algorithm that utilizes canopy reflectance models in both classification and biophysical characteristics estimation. Using the algorithm, we have classified a  $10,000 \text{ km}^2$  area of the southern boreal forest in central Saskatchewan and estimated the biomass density for the dominant land cover type in the circumpolar boreal ecosystem, wetland black spruce.

Our classification accuracies are equivalent to those obtained with conventional statistically based algorithms but, more importantly, should be more robust over larger areas since the physically based approach can account directly for the effects on class signatures and surface reflectance of seasonal growth patterns and variations in illumination and viewing conditions (topography, Sun angle). Furthermore, we can predict a priori which spectral regions are likely confusion regions, i.e., where the class spectral trajectories intersect. We demonstrate the importance of misclassification in inflating BMD estimation error using an algorithm that relates reflectance to canopy cover and ultimately to BMD. The mean square difference for the correctly classified pixels is  $2.73 \text{ kg m}^{-2}$  and for the misclassified pixels  $3.96 \text{ kg m}^{-2}$ . We suggest that in advanced versions of this algorithm, Bayesian methods be used in conjunction with canopy reflectance models to generate parametric multispectral distribution functions to minimize the effect of misclassification on BMD error. In addition, improvements could incorporate the use of multitemporal, multiangle, and nonspectral data to resolve spectral confusion among classes.

The physically based approach represents an improvement over purely statistically based classification approaches in at least three ways: (1) it permits highly nonlinear multispectral class distribution functions to be accurately characterized, (2) classifier “training” is simplified since only “end member” reflectance values are required (as opposed to the statistically representative sample required for maximum likelihood), and (3) signature variations due to view, illumination angles, topography, and varying environmental conditions can be accounted for physically.

We have found that for conifers, in particular black spruce, a convenient natural relationship exists between height and volumetric density that renders the biomass density for black spruce stands independent of tree height and a function only of shadow or sunlit canopy fraction. This important fact greatly simplifies the estimation of biomass density from optical data since tree height is a difficult parameter to estimate. How broadly applicable this relation is in terms of other canopy types is not known.

## Appendix: Allometric conditions for biomass density to be linearly related to sunlit canopy fraction

The volumetric biomass density  $\rho_b$  for a single crown is given by  $\text{BM}/V$ , where BM is the biomass (kilogram) for a crown whose “envelope” occupies a volume  $V$  (cubic meter). For example, a conical crown with a base of diameter  $w$  and height  $h$  has an envelope volume equal to  $(\pi/12)hw^2$ . Allometric measurements of black spruce canopies in both the Superior National Forest and the BOREAS demonstrate that (1)  $w$  is proportional to the bole diameter at breast height (dbh),  $w = k_1(\text{dbh})$ ; and (2) BM is proportional to  $(\text{dbh})^2$ ,  $\text{BM} = k_2(\text{dbh})^2$ .

These two conditions make the volumetric mass density inversely proportional to tree height since

$$\text{BM} = k_2(\text{dbh})^2 = (w)^2 k_2 / (k_1)^2 = kw^2 \quad (\text{A1})$$

therefore

$$\rho_b = \text{BM}/V = kw^2 / [(\pi/12)hw^2] = (12k/\pi)h^{-1} \quad (\text{A2})$$

When allometric conditions 1 and 2 are satisfied, shorter trees must be denser trees requiring BMD to be independent

of tree height and a function solely of the sunlit canopy fraction. Then from (6) and (A2) in the main body,

$$\text{BMD} = \rho_b(C/3f)h = (12k/\pi)(C/3f) = (4k/\pi f)C, \quad (\text{A3})$$

$k$  and  $f$  can be determined from allometric data;  $f$  is the fraction of sunlit to total canopy fraction that can be determined from the conical geometry of the spruce tree and their  $h/w$  ratio. For black spruce in both the Superior National Forest and the BOREAS study area,  $h/w$  is about 7, and from solid geometry,  $f$  is given by 0.52; thus  $k_1$  is 14.3,  $k_2$  is 2833 kg/m<sup>2</sup>, and  $k$  is 14 kg/m<sup>2</sup>. From (A3), BMD is given by

$$\text{BMD} = 34.4 C \text{ (kg/m}^2\text{)} \quad (\text{A4})$$

## Notation

AVHRR	advanced very high resolution radiometer.
BMD	biomass density.
BOREAS	Boreal Ecosystem-Atmosphere Study.
EOS AM	Earth Observation System morning platform.
FASIR	fourier-adjustment, solar zenith angle corrected, interpolated, reconstructed.
FIFE	First International Satellite Land Surface Climatology Project (ISLSCP) Field Experiment.
FLIM	forest-light interaction model.
Fpar	fraction of absorbed photosynthetically active radiation.
GCM	global circulation model.
HAPEX	Hydrological Atmospheric Pilot Experiment.
ISLSCP	International Satellite Land Surface Climatology Project.
LAD	leaf angle distribution.
LAI	leaf area index.
LOP	leaf optical properties.
Landsat	land satellite.
MIR	middle infrared.
MISR	multiangle imaging spectroradiometer.
MODIS	moderate resolution imaging spectrometer.
NDVI	normalized difference vegetation index.
NIR	near infrared.
R	surface reflectance.
SAIL	scattering from arbitrarily inclined leaves.
TM	Thematic Mapper.

## References

- Badhwar, G. D., J. G. Carnes, and W. W. Austin, Use of Landsat-derived temporal profiles for corn-soybeans feature extraction and classification, *Remote Sens. Environ.*, 12, 57–59, 1982.
- Ball, G. H., and D. J. Hall, A Clustering Technique for Summarizing Multivariate Data, *Behavioral Sciences*, 12(2), 153–155, 1967.
- Black, T. A., et al., Annual cycles of water vapor and carbon dioxide fluxes in and above a boreal aspen stand, *Global Change Biol.*, 2, 219–299, 1996.
- Frolking, S., et al., Modeling temporal variability in the carbon balance of a spruce/moss boreal forest, *Global Change Biol.*, 2, 343–366, 1996.
- Goel, N. S., Models of vegetation canopy reflectance and their use in estimation of biophysical parameters from reflectance data, *Remote Sens. Rev.*, 4, 1–121, 1988.
- Goel, N. S., and T. Grier, Estimation of canopy parameters for inhomogeneous vegetation canopies from reflectance data, III, TRIM: A model for radiative transfer in heterogeneous three-dimensional canopies, *Remote Sens. Environ.*, 25, 255–293, 1988.
- Goel, N. S., and R. L. Thompson, Inversion of vegetation canopy reflectance models for estimating agronomic variables, V, Estimation of LAI and average leaf angle using measured canopy reflectances, *Remote Sens. Environ.*, 16, 69–85, 1984.
- Hall, F. G., and G. D. Badhwar, Signature-extendable technology: Global space-based crop recognition, *IEEE Trans. Geosci. Remote Sens.*, GE-25, 93–103, 1987.
- Hall, F. G., D. B. Botkin, D. E. Strelbel, K. D. Woods, and S. J. Goetz, Forest succession and dynamics from remote sensing, *Ecology*, 72(2), 628–640, 1991.
- Hall, F. G., K. F. Huemmrich, D. E. Strelbel, S. J. Goetz, J. E. Nickelson, and K. D. Woods, Biophysical, morphological, canopy optical property, and productivity data from the Superior National Forest, *NASA Tech. Memo. 104568*, 1992.
- Hall, F. G., Y. E. Shimabukuro, and K. F. Huemmrich, Remote sensing of forest biophysical structure using mixture decomposition and geometric reflectance models, *Ecol. Appl.*, 5(4), 993–1013, 1995.
- Hall, F. G., D. R. Peddle, and E. F. LeDrew, Remote sensing of biophysical variables in boreal forest stands of *Picea Mariana*, *Int. J. Remote Sens.*, 17(15), 3077–3081, 1996.
- Horowitz, H. M., J. T. Lewis, and A. P. Pentland, Estimating proportions of objects from multispectral scanner data, final report, NASA contract NAS9-14123, NASA CR 141826, 1975.
- Huemmrich, K. F., A simple addition to the SAIL model to describe discontinuous canopy reflectance: The GeoSail model, *Remote Sens. Environ.*, in press, 1997.
- Jasinski, M. F., and P. S. Eagleson, Estimation of subpixel vegetation cover using red-infrared scatter grams, *IEEE Trans. Geosci. Remote Sens.*, 28(2), 253–267, 1990.
- Kettig, R. L., and D. A. Landgrebe, Classification of spectral image data by extraction and classification of homogeneous objects, *IEEE Transactions of Geoscience Electronics*, 14, 19–25, 1976.
- Larsen, J. A., *The Boreal Ecosystem*, pp. 328–329, Academic, San Diego, Calif., 1980.
- Li, X., and A. H. Strahler, Geometrical-optical modeling for a conifer forest canopy, *IEEE Trans. Geosci. Remote Sens.*, GE-23, 705–721, 1985.
- Lloyd, D., A phenological classification of terrestrial vegetation cover using shortwave vegetation index imagery, *Int. J. Remote Sens.*, 11(12), 2269–2279, 1990.
- Loechel, S. E., C. L. Walthall, E. Brown de Colstoun, J. Chen, B. L. Markham, and J. Miller, Variability of boreal forest reflectances as measured from a helicopter platform, *J. Geophys. Res.*, this issue.
- Mather, P. M., Preprocessing of training data for multispectral image classification, in paper presented at the 13th Annual Conference on Advances in Digital Image Processing, Remote Sens. Soc., Nottingham, England, 1987.
- Novo, E. M. M., and Y. E. Shimabukuro, Spectral mixture analysis of inland tropical waters, *Int. J. Remote Sens.*, 15(6), 1351–1356, 1994.
- Sellers, P. J., F. G. Hall, G. Asrar, D. E. Strelbel, and R. E. Murphy, The first ISLSCP field experiment (FIFE), *Bull. Am. Meteorol. Soc.*, 1(69), 22–27, 1988.
- Sellers, P. J., F. G. Hall, G. Asrar, D. E. Strelbel, and R. E. Murphy, An overview of the First International Satellite Land Surface Climatology Project (ISLSCP) Field Experiment (FIFE), *J. Geophys. Res.*, 97, 18,345–18,371, 1992.
- Sellers, P. J., S. O. Los, C. J. Tucker, C. O. Justice, D. A. Dazlich, G. J. Collatz, and D. A. Randall, A global 1-“degree” by 1-“degree” NDVI data set for climate studies, 2, The generation of global fields of terrestrial biophysical parameters from the NDVI, *Int. J. Remote Sens.*, 15, 3519–3545, 1994.
- Sellers, P., et al., The Boreal Ecosystem-Atmosphere Study (BOREAS): An overview and early results from the 1994 field year, *Bull. Am. Meteorol. Soc.*, 76(9), 1549–1577, 1995.
- Settle, J. J., Contextual classification of remotely sensed data, in *Proceedings on Mathematics and Its Applications in Remote Sensing*, edited by S. R. Brooks, Oxford Univ. Press, New York, 1989.
- Shimabukuro, Y. E., and J. A. Smith, Fraction images derived from Landsat TM and MSS data for monitoring reforested areas, *Can. J. Remote Sens.*, 21(1), 67–74, 1995.
- Shimabukuro, Y. E., B. N. Holben, and C. J. Tucker, Fraction images derived from NOAA AVHRR data for studying the deforestation in the Brazilian Amazon, Cover, *Int. J. Remote Sens.*, 15(3), 517–520, 1994.
- Smith, O. S., S. L. Ustin, J. B. Adams, and A. R. Gillespie, Vegetation in deserts, I, A regional measure of abundance from multispectral images, *Remote Sens. Environ.*, 31, 1–26, 1990a.
- Smith, O. S., S. L. Ustin, J. B. Adams, and A. R. Gillespie, Vegetation

- in deserts, II, A regional measure of abundance from multispectral images, *Remote Sens. Environ.*, **31**, 1–26, 1990b.
- Steyaert, L. T., F. G. Hall, and T. R. Loveland, Land cover mapping, fire regeneration, and scaling studies in the Canadian boreal forest with 1-km AVHRR and Landsat TM data, *J. Geophys. Res.*, this issue.
- Strebel, D. E., D. R. Landis, K. F. Huemmrich, and B. W. Meeson, Collected data of the First ISLSCP Field Experiment, in *Surface Observations and Non-Image Data Sets*, vol. 1, CDROM, Field Exp. Data Arch., Oak Ridge Natl. Lab., Oak Ridge, Tenn., 1994.
- Swain, P. H., and S. M. Davis, *Remote Sensing: The Quantitative Approach*, McGraw-Hill, New York, 1978.
- Townshend, J. R. G., C. O. Justice, W. Li, C. Gurney, and J. McManus, Global land cover classification by remote sensing: Present capabilities and future possibilities, *Remote Sens. Environ.*, **35**, 243–256, 1991.
- Verhoef, W., Light scattering by leaf layers with application to canopy reflectance modeling: The SAIL model, *Remote Sens. Environ.*, **16**, 125–141, 1984.
- F. G. Hall and K. Huemmrich, NASA Goddard Space Flight Center, Code 923, Greenbelt, MD 20771. (e-mail: fghall@ltpmail.gsfc.nasa.gov)
- D. Knapp, Hughes STX, 7701 Greenbelt Rd., Suite 400, Greenbelt, MD 20770.

(Received January 30, 1997; revised September 4, 1997; accepted September 4, 1997.)